UNIVERSITY OF STRATHCLYDE

DEPARTMENT OF
MATHEMATICS AND STATISTICS

A GROWTH-FRAGMENTATION MODEL OF HYPHAL GROWTH AND BRANCHING OF THE FILAMENTOUS BACTERIA *STREPTOMYCES COELICOLOR*.

by

Katherine Broadfoot

201009137

BSc Hons Mathematics

2014

Statement of work in project

The work contained in this project is that of the author and where material from other sources has been incorporated full acknowledgement is made.

Signed .....

Print Name .....

Date .....

Supervised by Dr John A. MacKenzie.

Contents

1 Introduction

Streptomyces is an antibiotic producing bacteria which is the source of the majority of antibiotics currently in use [1]. In particular, the *Streptomyces coelicolor* (*S. coelicolor*) genome is of particular interest as it has been fully sequenced [2] and has a range of secondary metabolites including antibiotic production. *S. coelicolor* is formed by a branching filamentous network (as shown in Fig. 1), known as a mycelium, which is similar to that produced by filamentous fungi [3]. Many other branching structures (e.g. roots of plants and neuron networks) occur in biology, and simple characterisation of these systems is highly sought after.

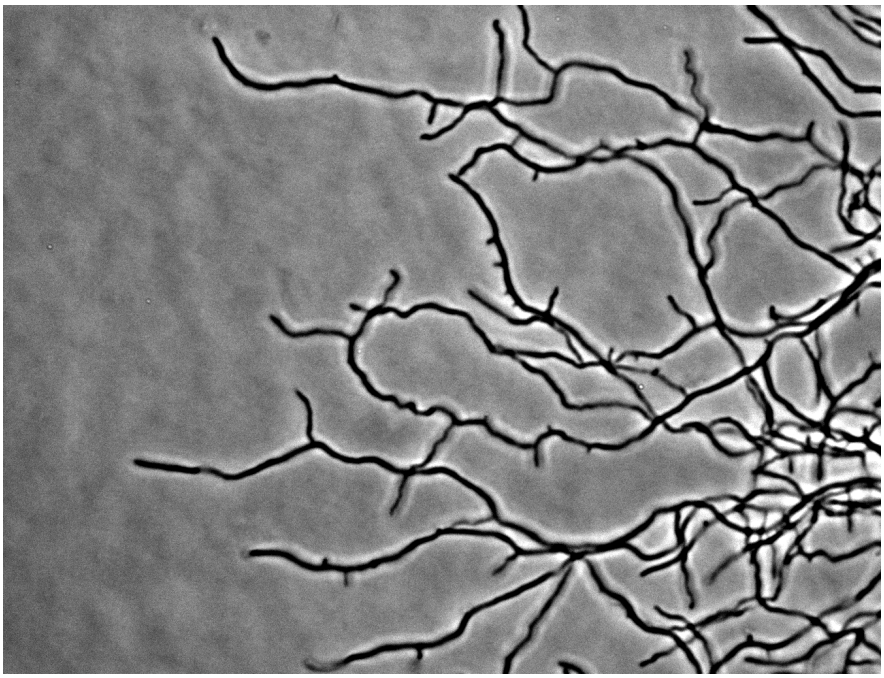

Figure 1: Example of hyphal growth in *S.coelicolor* provided by Dr Paul Herron, SIPBS, University of Strathclyde.

The protein DivIVA has been found to be essential for growth of *S.coelicolor* and to indicate future branch positions [4]. The monomeric form of DivIVA binds together to form clusters (or foci) at the hyphal tip. These clusters then grow in size due to this binding process and travel with the tip as the mycelium grows. When the cluster size reaches x_{split}, it may split into two new clusters; the parent cluster of size $x_{\text{split}} - x_0$, which will continue to grow and travel with the tip as

before the splitting event, and the daughter of size x_0 which will remain at the location of the split. The daughter cluster will grow until it reaches size x_{branch} and will then be able to form a branch at this location, becoming the parent cluster of this new tip. However, experimental data suggests that a cluster will not always split immediately after reaching x_{split}, and so a probability of splitting is assigned after this size has been reached [5],[6]. This behaviour is shown in Fig. 2 below.

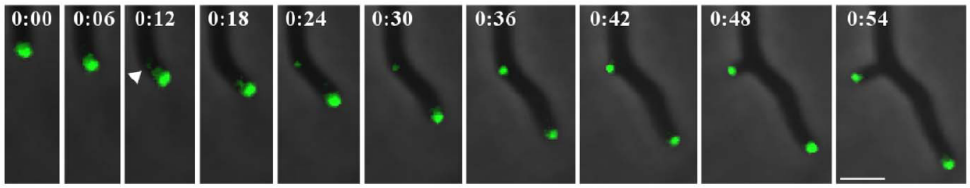

Figure 2: Example of hyphal growth and branching, with cluster at the hyphal tip which splits at 0:12. The parent cluster continues to travel with the hyphal tip and the daughter cluster grows until forming a branch at 0:48 and then travels with this new tip [5].

The minimal model proposed by Howard et al [5] uses experimental data to estimate the parameters involved in this process. In particular the binding parameter, which is taken as $\beta = 7 \times 10^{-5} s^{-1}$, represents the rate at which monomeric DivIVA binds onto the clusters, the minimum cluster size for splitting is taken to be $x_{\text{split}} = 10^4$ molecules and the probability of cluster splitting per unit time is $\gamma = 10^{-3}\text{s}^{-1}$. The binding process is modelled as $\frac{dx}{dt} = \beta x$, where x is the cluster size, which results in exponential growth of the clusters.

This report will propose a growth-fragmentation model to describe the process described above and outline some properties, and the significance of, the zeroth and first moments of this model. A numerical method for solving the growth-fragmentation model will then be proposed and used to evolve the system, and the accuracy of the numerical method will then be tested by comparing the numerical solution to a known analytical solution. We can then apply the numerical method to the described biological problem. The computational results will then be dis-

cussed, in particular the existence of stable size distributions and the necessary parameter values to achieve a biologically sound result. Stable size distributions are of interest as their existence has been shown for growth-fragmentation models [7] and they allow simple characterisation of the model for comparison with experimental results.

2 Growth-fragmentation model

This splitting of DivIVA clusters can be described using growth-fragmentation equations, which are applied to many different areas such as modelling of: cell division [10], neuron networks [11] and protein polymerization [12]. However, we believe these growth-fragmentation equations have not been used to model a branching network such as that produced by the splitting process of DivIVA in *S.coelicolor*. We will let the number density of clusters of size x at time t be denoted by $n(x,t)$. The process of cluster growth and splitting will be modelled using the following mass-balance equation [7], [8]:

$$\frac{\partial}{\partial t}n(x,t) = \underbrace{-c\frac{\partial}{\partial x}\left(g(x)n(x,t)\right)}_{\text{Growth term}} \underbrace{-s(x)n(x,t) + 2\int_0^\infty s(y)p(x,y)n(y,t)dy}_{\text{Splitting terms}}, \quad (1)$$

where $c > 0$ is a constant, $g(x) > 0$ and $n(x,0) = n^0(x)$. We also assume that there is no flux at $x = 0$ and that $n(x,t)$ decreases sufficiently fast that there is also no flux as $x \to \infty$, so that

$$g(0)n(0,t) = \lim_{x\to\infty} g(x)n(x,t) = 0. \quad (2)$$

The division rate of clusters of size y is given by $s(y)$ and the growth rate by $cg(x)$. The probability of a cluster of size y splitting into clusters of size x and $y - x$ is given by $p(x,y)$, and the following assumptions are made about this quantity [9]:

$$p(x,y) = 0, \ \forall x > y, \quad (3)$$

$$\int_0^\infty p(x,y)dx = 1, \quad (4)$$

$$p(x, y) = p(y - x, y). \tag{5}$$

We will frequently consider the zeroth moment of the number density $n(x, t)$,

$$M_0(t) = \int_0^\infty n(x, t)dx,$$

which represents the total number of clusters in the system, and the first moment,

$$M_1(t) = \int_0^\infty xn(x, t)dx,$$

which represents the total mass of the system.

In the absence of splitting, the total number of clusters will not change, and hence the zeroth moment will be constant. If $s(x) = 0$, then (1) simplifies to

$$\frac{\partial}{\partial t}n(x, t) = -c\frac{\partial}{\partial x}\left(g(x)n(x, t)\right). \tag{6}$$

To show that the zeroth moment, M_0, is constant, consider

$$\frac{dM_0}{dt} = \frac{d}{dt}\int_0^\infty n(x, t)dx = \int_0^\infty \frac{\partial}{\partial t}n(x, t)dx.$$

Using (6), we have

$$\begin{aligned}\frac{dM_0}{dt} &= -c\int_0^\infty \frac{\partial}{\partial x}\left(g(x)n(x, t)\right)dx \\ &= -c\left[g(x)n(x, t)\right]_0^\infty.\end{aligned}$$

Using the boundary conditions (2), we therefore have

$$\frac{dM_0}{dt} = 0,$$

and hence $M_0(t) = M_0(0)$. Therefore, the zeroth moment (number of clusters) is conserved as expected.

Similarly, in the absence of growth the clusters will continue to split but there will be no increase in the total mass of the system. Therefore in this situation

the first moment should remain constant.

To show this, the integral $\int_0^\infty xp(x,y)dx$ must first be evaluated. Using (3) and integration by parts we have

$$\begin{aligned}
\int_0^\infty xp(x,y)dx &= \int_0^y xp(x,y)dx \\
&= \left[x\int_0^x p(s,y)ds\right]_0^y - \int_0^y\int_0^x p(s,y)dsdx \\
&= y - \int_0^y\int_s^y p(s,y)dxds \\
&= y - \int_0^y \left(\int_s^y dx\right) p(s,y)ds \\
&= y - \int_0^y (y-s)p(y-s,y)ds \\
&= y - \int_0^\infty xp(x,y)dx.
\end{aligned}$$

Therefore

$$\int_0^\infty xp(x,y)dx = \frac{y}{2}. \tag{7}$$

In the absence of growth, (1) simplifies to

$$\frac{\partial}{\partial t}n(x,t) = \underbrace{-s(x)n(x,t)}_{\text{Death term}} + \underbrace{2\int_0^\infty s(y)p(x,y)n(y,t)dy}_{\text{Birth term}}. \tag{8}$$

Therefore,

$$\begin{aligned}
\frac{dM_1}{dt} &= \frac{d}{dt}\int_0^\infty xn(x,t)dx \\
&= \int_0^\infty x\frac{\partial}{\partial t}n(x,t)dx \\
&= \int_0^\infty x\left(-s(x)n(x,t) + 2\int_0^\infty s(y)p(x,y)n(y,t)dy\right)dx
\end{aligned}$$

$$
\begin{aligned}
&= -\int_0^\infty xs(x)n(x,t)dx + 2\int_0^\infty x\int_0^\infty s(y)p(x,y)n(y,t)dydx \\
&= -\int_0^\infty xs(x)n(x,t)dx + 2\int_0^\infty\int_0^\infty xs(y)p(x,y)n(y,t)dydx \\
&= -\int_0^\infty xs(x)n(x,t)dx + 2\int_0^\infty\int_0^\infty \frac{x}{y}ys(y)p(x,y)n(y,t)dydx \\
&= -\int_0^\infty xs(x)n(x,t)dx + 2\int_0^\infty\int_0^\infty \frac{x}{y}ys(y)p(x,y)n(y,t)dxdy \\
&= -\int_0^\infty ys(y)n(y,t)dy + 2\int_0^\infty ys(y)n(y,t)dy\int_0^\infty \frac{x}{y}p(x,y)dx \\
&= \int_0^\infty ys(y)n(y,t)dy\left(\frac{2}{y}\int_0^\infty xp(x,y)dx - 1\right) \\
&= \int_0^\infty ys(y)n(y,t)dy\left(\frac{2}{y}\left(\frac{y}{2}\right) - 1\right) \\
&= 0,
\end{aligned}
$$

and therefore the first moment (total mass) is preserved in the absence of growth.

3 Numerical discretization of model

Although the growth fragmentation equation (1) is linear in n, it is not easy to find analytical solutions for general functions $g(x), s(y)$and $p(x,y)$. It is therefore advantageous to use an appropriate numerical method to solve the system.

To solve (1) numerically, we consider the application of a so called sectional method. First the total size range of the clusters, $[v_{\min}, v_{\max}]$, is partitioned into smaller size ranges, $[v_i, v_{i+1}]$ (the i^{th} section). All of the cluster sizes in this range are then represented by a single cluster size x_i, where $v_i < x_i < v_{i+1}$. A grid of this type is shown in Fig. 3.

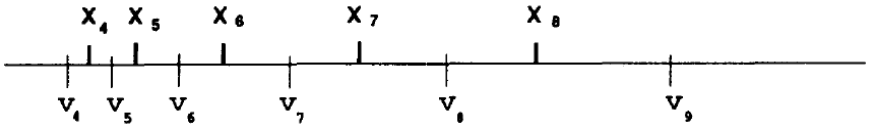

Figure 3: General grid to be used with numerical technique, where $x_i = (v_i + v_{i+1})/2$ [13].

3.1 Fixed pivot method for binary splitting

We first consider only the splitting terms, as in (8). When a cluster is created through splitting, the cluster size does not necessarily correspond exactly to one of the grid points, x_i. This is dealt with by distributing $a(x, x_i)$ of the clusters in (x_i, x_{i+1}) to the grid point x_i and $b(x, x_i)$ of the clusters in (x_{i-1}, x_i) to x_i, such that the zeroth and first moments are preserved exactly. Therefore

$$\int_{v_i}^{v_{i+1}} dx = \int_{x_i}^{x_{i+1}} a(x, x_i)dx + \int_{x_{i-1}}^{x_i} b(x, x_i)dx, \tag{9}$$

and hence,

$$\begin{aligned}
\int_{v_i}^{v_{i+1}} n(x,t)dx &= \int_{x_i}^{x_{i+1}} a(x, x_i)n(x,t)dx + \int_{x_{i-1}}^{x_i} b(x, x_i)n(x,t)dx \\
&= \int_{x_i}^{x_{i+1}} a(x, x_i)n(x,t)dx + \int_{x_i}^{x_{i+1}} b(x, x_{i+1})n(x,t)dx \\
&= \int_{x_i}^{x_{i+1}} \left(a(x, x_i) + b(x, x_{i+1})\right) n(x,t)dx \\
\Rightarrow \int_0^{\infty} n(x,t)dx &= \int_0^{\infty} \left(a(x, x_i) + b(x, x_{i+1})\right) n(x,t)dx.
\end{aligned}$$

So for the zeroth moment to be preserved, we require

$$a(x, x_i) + b(x, x_{i+1}) = 1. \tag{10}$$

Similarly,

$$\begin{aligned}
\int_{v_i}^{v_{i+1}} xn(x,t)dx &= \int_{x_i}^{x_{i+1}} x_i a(x, x_i)n(x,t)dx + \int_{x_{i-1}}^{x_i} x_i b(x, x_i)n(x,t)dx \\
&= \int_{x_i}^{x_{i+1}} x_i a(x, x_i)n(x,t)dx + \int_{x_i}^{x_{i+1}} x_{i+1} b(x, x_{i+1})n(x,t)dx \\
&= \int_{x_i}^{x_{i+1}} \left(x_i a(x, x_i) + x_{i+1} b(x, x_{i+1})\right) n(x,t)dx \\
\Rightarrow \int_0^{\infty} xn(x,t)dx &= \int_0^{\infty} \left(x_i a(x, x_i) + x_{i+1} b(x, x_{i+1})\right) n(x,t)dx,
\end{aligned}$$

and therefore for the first moment to be preserved, we must have

$$x_i a(x, x_i) + x_{i+1} b(x, x_{i+1}) = x. \tag{11}$$

From (10), we have

$$b(x, x_{i+1}) = 1 - a(x, x_i). \tag{12}$$

Substituting into (11), we get

$$\begin{aligned} &a(x, x_i)x_i + (1 - a(x, x_i))\, x_{i+1} = x \\ \Rightarrow\ &a(x, x_i)(x_i - x_{i+1}) = x - x_{i+1}, \end{aligned}$$

therefore

$$\begin{aligned} a(x, x_i) &= \frac{x - x_{i+1}}{x_i - x_{i+1}} \\ &= \frac{x_{i+1} - x}{x_{i+1} - x_i}. \end{aligned} \tag{13}$$

Substituting (13) back into (12), we set

$$b(x, x_{i+1}) = \frac{x - x_i}{x_{i+1} - x_i}. \tag{14}$$

If we assume that the cluster sizes are represented solely by the grid points, x_i, the number density can be expressed approximately as:

$$n(x, t) \approx \sum_{k=1}^{M} N_k(t)\delta(x - x_k), \tag{15}$$

where $\delta(x - x_k)$ is Dirac's delta function such that $\delta(x - x_k) = 0$, for all $x \neq x_k$ and

$$N_i(t) = \int_{v_i}^{v_{i+1}} n(x, t)dx \tag{16}$$

is the number of clusters in the size range (v_i, v_{i+1}).

Integrating (8) from v_i to v_{i+1} we get

$$\begin{aligned} &\int_{v_i}^{v_{i+1}} \frac{\partial}{\partial t} n(x, t)dx = -\int_{v_i}^{v_{i+1}} s(x)n(x, t)dx + 2\int_{v_i}^{v_{i+1}}\int_{0}^{\infty} s(y)p(x, y)n(y, t)dydx \\ \Rightarrow\ &\frac{d}{dt}\int_{v_i}^{v_{i+1}} n(x, t)dx \approx -\int_{v_i}^{v_{i+1}} s(x)\sum_{k=1}^{M} N_k(t)\delta(x - x_k)dx \end{aligned}$$

$$
\begin{aligned}
&+ 2 \int_{x_i}^{x_{i+1}} a(x, x_i) \int_0^{\infty} s(y) p(x, y) n(y, t) dy dx \\
&+ 2 \int_{x_{i-1}}^{x_i} b(x, x_i) \int_0^{\infty} s(y) p(x, y) n(y, t) dy dx \\
\Rightarrow \frac{dN_i(t)}{dt} &\approx -N_i(t) s(x_i) + 2 \int_{x_i}^{x_{i+1}} a(x, x_i) \int_0^{\infty} s(y) p(x, y) \sum_{k=1}^{M} N_k(t) \delta(y - x_k) dy dx \\
&+ 2 \int_{x_{i-1}}^{x_i} b(x, x_i) \int_0^{\infty} s(y) p(x, y) \sum_{k=1}^{M} N_k(t) \delta(y - x_k) dy dx \\
&= -N_i(t) s(x_i) + 2 \sum_{k=1}^{M} N_k(t) s(x_k) \int_{x_i}^{x_{i+1}} a(x, x_i) p(x, x_k) dx \\
&+ 2 \sum_{k=1}^{M} N_k(t) s(x_k) \int_{x_{i-1}}^{x_i} b(x, x_i) p(x, x_k) dx \\
&= \sum_{k=i}^{M} N_k(t) s(x_k) \left(2 \int_{x_i}^{x_{i+1}} a(x, x_i) p(x, x_k) dx + 2 \int_{x_{i-1}}^{x_i} b(x, x_i) p(x, x_k) dx \right) - N_i(t) s(x_i) \\
&= \sum_{k=i}^{M} N_k(t) s(x_k) \eta_{i,k} - N_i(t) s(x_i), \qquad (17)
\end{aligned}
$$

where

$$
\begin{aligned}
\eta_{i,k} &= 2 \int_{x_i}^{x_{i+1}} a(x, x_i) p(x, x_k) dx + 2 \int_{x_{i-1}}^{x_i} b(x, x_i) p(x, x_k) dx \\
&= 2 \int_{x_i}^{x_{i+1}} \frac{x_{i+1} - x}{x_{i+1} - x_i} p(x, x_k) dx + 2 \int_{x_{i-1}}^{x_i} \frac{x - x_{i-1}}{x_i - x_{i-1}} p(x, x_k) dx. \qquad (18)
\end{aligned}
$$

In the section on numerical results, the midpoint quadrature rule has been used to approximate the integrals in (18).

3.2 Modified upwind scheme for growth

Similarly to when dealing with the splitting event, we consider only the effect of growth, as in (6), and aim to accurately evolve the zeroth and first moments using a numerical scheme. As we have taken $g(x) = x$, this describes the advection

equation and hence an upwind scheme is an appropriate numerical method for this problem. If we integrate (6) from v_i to v_{i+1}, then

$$\int_{v_i}^{v_{i+1}} \frac{\partial}{\partial t} n(x,t)dx = -\int_{v_i}^{v_{i+1}} \frac{\partial}{\partial x}\left(cg(x)n(x,t)\right)dx$$
$$\Rightarrow \frac{dNi}{dt} = -[cg(x)n(x,t)]_{v_i}^{v_{i+1}} = -c\left(g(v_{i+1})n(v_{i+1},t) - g(v_i)n(v_i,t)\right). \tag{19}$$

Here, the use of an upwind differencing scheme rather than e.g. a central differencing scheme is important. We wish to evaluate $n(v_i,t)$ at one of the grid points, rather than at a section boundary, v_i. To acheive this, information is taken form the upwind direction, opposite to the direction of advective flow. Hence, as $c > 0$ and $g(x) > 0$, we approximate $n(v_i,t)$ by $n(x_{i-1},t)$ (i.e. at the grid point to the left of the section boundary we are considering). Therefore, substituting $n(v_i,t) = n(x_{i-1},t)$ into (19), we get

$$\frac{dN_i}{dt} = -c(g(v_{i+1})n_i(t) - g(v_i)n_{i-1}(t)), \tag{20}$$

where $n_i(t) = n(x_i,t)$.

To obtain an approximation for $n_i(t)$, consider the definition of $N_i(t)$:

$$N_i(t) = \int_{v_i}^{v_{i+1}} n(x,t)dx \approx \int_{v_i}^{v_{i+1}} n(x_i,t)dx$$
$$= n(x_i,t)\int_{v_i}^{v_{i+1}} dx = (v_i - v_{i+1})n_i(t),$$

and hence

$$n_i(t) \approx \frac{N_i(t)}{v_{i+1} - v_i}. \tag{21}$$

We can now substitute (21) into (20), giving

$$\frac{dN_i}{dt} \approx -c\left(\frac{g(v_{i+1})N_i(t)}{v_{i+1} - v_i} - \frac{g(v_i)N_{i-1}(t)}{v_i - v_{i-1}}\right). \tag{22}$$

We now consider the zeroth moment,

$$M_0(t) = \int_0^\infty n(x,t)dx \approx \sum_{i=1}^{L}\int_{v_i}^{v_{i+1}} n(x,t)dx$$

$$= \sum_{i=1}^{L} N_i(t),$$

where L is such that $v_{L+1} = v_{\max}$. Therefore,

$$\begin{aligned}
\frac{dM_0}{dt} &= \sum_{i=1}^{L} \frac{dN_i}{dt} \\
&= \sum_{i=1}^{L} -c \left(\frac{g(v_{i+1})N_i(t)}{v_{i+1} - v_i} - \frac{g(v_i)N_{i-1}(t)}{v_i - v_{i-1}} \right) \\
&= -c \left(\frac{-g(v_1)N_0}{v_1 - v_0} + \frac{g(v_{L+1})N_L}{v_{L+1} - v_L} \right).
\end{aligned}$$

The zeroth moment is expected to evolve according to

$$\frac{dM_0}{dt} = -cg(v_{L+1})n(v_{L+1}, t) + cg(v_1)n(v_1, t). \tag{23}$$

Therefore, by using the approximation (21) and evaluating the number density at the right section boundary,

$$\begin{aligned}
\frac{dM_0}{dt} &= -\frac{cg(v_{L+1})N_L}{v_{L+1} - v_L}) + \frac{cg(v_1)N_0}{v_1 - v_0} \\
&\approx -cg(v_{L+1})n_L(t) + cg(v_1)n_0(t) \\
&\approx -cg(v_{L+1})n(v_{L+1}, t) + cg(v_1)n(v_1, t),
\end{aligned} \tag{24}$$

and therefore the zeroth moment evolves as expected, when the number density is evaluated at the right boundary point of the section.

However, this numerical approximation will not accurately evolve the first moment. To show this, we must first approximate the first moment:

$$\begin{aligned}
M_1(t) &= \int_0^{\infty} xn(x, t)dx \\
&\approx \sum_{i=1}^{L} \int_{v_i}^{v_{i+1}} x_i n(x, t)dx \\
&= \sum_{i=1}^{L} x_i N_i(t).
\end{aligned}$$

Therefore,

$$\begin{aligned}
\frac{dM_1}{dt} &\approx \sum_{i=1}^{L} x_i \frac{dN_i}{dt} \\
&= \sum_{i=1}^{L} -cx_i \left(\frac{g(v_{i+1})N_i(t)}{v_{i+1}-v_i} - \frac{g(v_i)N_{i-1}(t)}{v_i - v_{i-1}} \right) \\
&= \frac{cx_1 g(v_1)N_0(t)}{v_1 - v_0} - \frac{cx_L g(v_{L+1})N_L(t)}{v_{L+1}-v_L} + c\sum_{i=1}^{L-1} \frac{(x_{i+1}-x_i)g(v_{i+1})N_i(t)}{v_{i+1}-v_i} \\
&\approx cx_1 g(v_1)n_0(t) - cx_L g(v_{L+1})n_L(t) + c\sum_{i=1}^{L-1}(x_{i+1}-x_i)g(v_{i+1})n_i(t) \\
&\approx -cv_{L+1}g(v_{L+1})n(v_{L+1},t) + cv_1 g(v_1)n(v_1,t) + c\sum_{i=1}^{L-1}(x_{i+1}-x_i)g(v_{i+1})n_i(t),
\end{aligned}$$

by evaluating the number density at the right boundary point of the section, apart from in the summation. Hence, by substituting $x_i = (v_{i+1}+v_i)/2$,

$$\frac{dM_1}{dt} \approx -cv_{L+1}g(v_{L+1})n(v_{L+1},t) + cv_1 g(v_1)n(v_1,t) + c\sum_{i=1}^{L-1} \frac{v_{i+2}-v_i}{2} g(v_{i+1})n_i(t) \tag{25}$$

The first moment is expected to evolve according to

$$\frac{dM_1}{dt} = -cv_{L+1}g(v_{L+1})n(v_{L+1},t) + cv_1 g(v_1)n(v_1,t) + c\sum_{i=1}^{L-1}(v_{i+1}-v_i)g(v_{i+1})n_i(t). \tag{26}$$

Therefore, by comparing (25) with (26), we see that the first moment is not preserved using this scheme unless a uniform grid is being used (i.e. $v_{i+2} - v_i = 2(v_{i+1} - v_i)$).

To preserve both the zeroth and the first moments without the requirement for a uniform grid, it is necessary to use a modified upwind scheme[14], [15]:

$$\frac{dN_i}{dt} = cg(x_{i-1})\frac{N_{i-1}}{x_i - x_{i-1}} - cg(x_i)\frac{N_i}{x_{i+1}-x_i}. \tag{27}$$

To show that the zeroth moment is preserved for the modified scheme (27),

$$\frac{dM_0}{dt} = \sum_{i=1}^{L} \frac{dN_i}{dt}$$

$$
\begin{aligned}
&= \sum_{i=1}^{L} cg(x_{i-1}) \frac{N_{i-1}}{x_i - x_{i-1}} - cg(x_i) \frac{N_i}{x_{i+1} - x_i} \\
&= cg(x_0) \frac{N_0}{x_1 - x_0} - cg(x_L) \frac{n_L}{x_{L+1} - x_L} \\
&\approx cg(x_0) n_0 \frac{(v_1 - v_0)}{x_1 - x_0} - cg(x_L) n_L \frac{v_{L+1-v_L}}{x_{L+1} - x_L}.
\end{aligned}
$$

It is necessary here to use an assumption on ghost meshes, so that

$$
\begin{aligned}
x_{L+1} &= x_L + (v_{L+1} - v_L) \\
\Rightarrow x_{L+1} - x_L &= v_{L+1} - v_L,
\end{aligned}
$$

and $v_1 - v_0 = v_2 - v_1$, so that

$$
\begin{aligned}
x_0 &= x_1 - (v_1 - v_0) = x_1 - (v_2 - v_1) \\
\Rightarrow x_1 - x_0 &= v_1 - v_0.
\end{aligned}
$$

Therefore,

$$
\frac{dM_0}{dt} \approx cg(x_0) n(x_0, t) - cg(x_L) n(x_L, t),
$$

and by evaluating the growth and number density at the right boundary points of the section, we arrive at

$$
\frac{dM_0}{dt} \approx -cg(v_{L+1}) n(v_{L+1}, t) + cg(v_1) n(v_1, t). \tag{28}
$$

Therefore, by comparing (28) with the expected evolution of the zeroth moment (23), we once again see that the zeroth moment is preserved.

Similarly, for the first moment

$$
\begin{aligned}
\frac{dM_1}{dt} &\approx \sum_{i=1}^{L} x_i \frac{dN_i}{dt} \\
&= \sum_{i=1}^{L} cx_i \left(g(x_{i-1}) \frac{N_{i-1}}{x_i - x_{i-1}} - g(x_i) \frac{N_i}{x_{i+1} - x_i} \right) \\
&= \sum_{i=1}^{L} cx_i \left(g(x_{i-1}) \frac{n_{i-1}(v_i - v_{i-1})}{x_i - x_{i-1}} - g(x_i) \frac{n_i(v_{i+1} - v_i)}{x_{i+1} - x_i} \right) \\
&= cx_1 g(x_0) \frac{N_0}{x_1 - x_0} - cx_L g(x_L) \frac{N_L}{x_{L+1} - x_L} + \sum_{i=1}^{L-1} c(x_{i+1} - x_i) g(x_i) \frac{N_i}{x_{i+1} - x_i}
\end{aligned}
$$

$$= cx_1 g(x_0)\frac{N_0}{x_1 - x_0} - cx_L g(x_L)\frac{N_L}{x_{L+1} - x_L} + \sum_{i=1}^{L-1} cg(x_i)N_i$$

$$= cx_1 g(x_0)\frac{n_0(v_1 - v_0)}{x_1 - x_0} - cx_L g(x_L)\frac{n_L(v_{L+1} - v_L)}{x_{L+1} - x_L} + \sum_{i=1}^{L-1} cg(x_i)n_i(v_{i+1} - v_i).$$

If the assumption on ghost cells is used once again, so that $x_1 - x_0 = v_1 - v_0$, and $x_{L+1} - x_L = v_{L+1} - v_L$, and we again evaluate at the right boundary of the section, apart from x_1, which is evaluated at the left boundary of the section v_1 as in [14], then we arrive at

$$\frac{dM_1}{dt} \approx -cv_{L+1}g(v_{L+1})n(v_{L+1}, t) + cv_1 g(v_1)n(v_1, t) + c\sum_{i=1}^{L-1}(v_{i+1} - v_i)g(v_{i+1})n_i(t), \tag{29}$$

which clearly corresponds exactly to (26), the expected evolution of the first moment and therefore the first moment is preserved.

As the zeroth and first moments evolve as expected under the modified upwind scheme (27), it is an appropriate choice for numerically solving the growth terms in (1). To allow us to solve our original equation (1), the modified upwind scheme for growth (27) and fixed pivot method for binary splitting (17) must be combined.

3.3 Combined numerical method

To solve (1) the fixed pivot method for splitting and the modified upwind scheme for growth must be combined to give one numerical scheme

$$\frac{dN_i(t)}{dt} = \sum_{k=i}^{L} N_k(t)s(x_k)\eta_{i,k} - N_i(t)s(x_i) + c\left(\frac{g(x_{i-1})N_{i-1}(t)}{x_i - x_{i-1}} - \frac{g(x_i)N_i(t)}{x_{i+1} - x_i}\right), \quad i = 1, \cdots, L$$

$$\Rightarrow \frac{d\mathbf{N}}{dt} = A\mathbf{N}, \tag{30}$$

where

$$A = \begin{pmatrix} s_1(\eta_{1,1} - 1) - \frac{cg_1}{x_2 - x_1} & s_2\eta_{1,2} & \cdots & s_L\eta_{1,L} \\ \frac{cg_1}{x_2 - x_1} & s_2(\eta_{2,2} - 1) - \frac{cg_2}{x_3 - x_2} & \cdots & s_L\eta_{2,L} \\ 0 & \frac{cg_2}{x_3 - x_2} & \cdots & s_L\eta_{3,L} \\ \vdots & & & \vdots \\ 0 & 0 & \cdots & s_L(\eta_{L,L} - 1) - \frac{cg_L}{x_{L+1} - x_L} \end{pmatrix},$$

and $s_i = s(x_i)$, $g_i = g(x_i)$.

To show that the solution, $\mathbf{N}(t)$, of (30) is always non-negative with the choice of the matrix A as above, we consider the following result [16], [17]: "The solution of $\frac{d\mathbf{N}}{dt} = A\mathbf{N}$ is non-negative iff $a_{i,j} \geq 0$ for all $j \neq i$."

By considering the structure of the matrix A, this will clearly hold. For all $j < i-1$, $a_{i,j} = 0$; for $j = i-1$, $a_{i,j} = \frac{cg_{i-1}}{x_i - x_{i-1}} > 0$ as we have assumed $c > 0, g(x) > 0$ and $x_i - x_{i-1} > 0$; and finally for $j > i$, $a_{i,j} = s_j \eta_{i,j} \geq 0$. Therefore $a_{i,j} \geq 0$ for all $j \neq i$ and hence the solution of (30) is non-negative using the quoted result above. This shows one advantage of using an upwind scheme for the growth terms; with another choice of differencing scheme, this non-negativity would not be guaranteed as the negative term currently affecting the diagonal terms due to growth would instead act on one of the off-diagonal terms.

4 Results

The system of ordinary differential equations describing the evolution of N_i, given in (30) can be solved numerically. This has been implemented using MATLAB and the numerical solver ODE45.

4.1 Comparison of numerical method with analytical solutions of zeroth and first moments

To verify the accuracy of the numerical scheme proposed, the parameters have been chosen in such a way that analytical solutions of the zeroth and first moments are known. Hence, by comparing the exact values of the moments with those predicted using the numerical method, we can verify that the method is accurate. Taking $c = 1, g(x) = x, s(x) = 1$,

$$p(x, y) = \frac{x^2(y-x)^2\Gamma(6)}{y^5\Gamma(3)^2}, \tag{31}$$

where $\Gamma(x)$ is the gamma function. The grid used by the numerical method was generated on the interval $[v_{\min}, v_{\max}]$ so that

$$v_i = v_{\min} \left(\frac{v_{\max}}{v_{\min}} \right)^{\frac{i-1}{L}}. \tag{32}$$

Where $[v_{\min}, v_{\max}] = [10^{-6}, 300]$ for this problem. The kernel (31) is plotted in Fig. 4 and using the exponential initial condition $n(x, 0) = e^{-x}$, the analytical solution of the zeroth moment, $M_0(t) = M_0(0)e^t$ and the first moment, $M_1(t) = M_1(0)e^t$ [14] can be plotted alongside the numerical solutions.

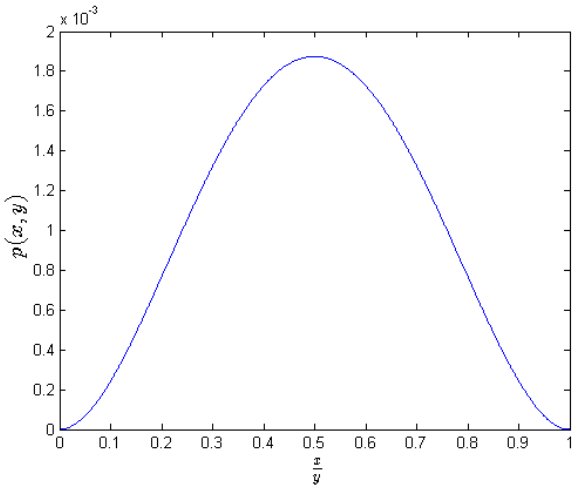

Figure 4: Breakage kernel, $p(x, y)$, given by (31) to be used for comparison of numerical and analytical solutions.

The comparison of the analytical and numerical solutions are shown below in Fig. 5. Clearly the method is performing well for the zeroth moment, but is slightly overestimating the analytical solution for the first moment. However, by increasing the number of grid points used in the numerical method, this error is reduced, as shown in Fig. 6.

By increasing the number of grid points from 60 to 300, the numerical solution is clearly converging towards the analytical solution. One possible source of this error is the use of the midpoint quadrature rule to evaluate the integrals involving $p(x, y)$ for the $\eta_{i,j}$ coefficients (18) in the fixed pivot method. This error could be removed if the $\eta_{i,j}$ can be calculated analytically, however this restricts the

possible choices for the breakage kernel.

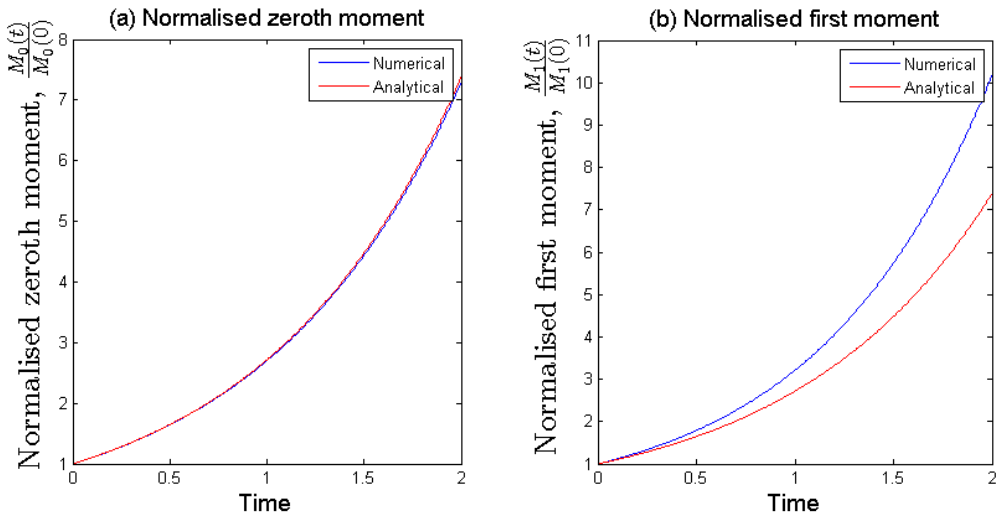

Figure 5: Comparison of the numerical and analytical solutions of the normalised (a) zeroth and (b) first moments using 60 grid points.

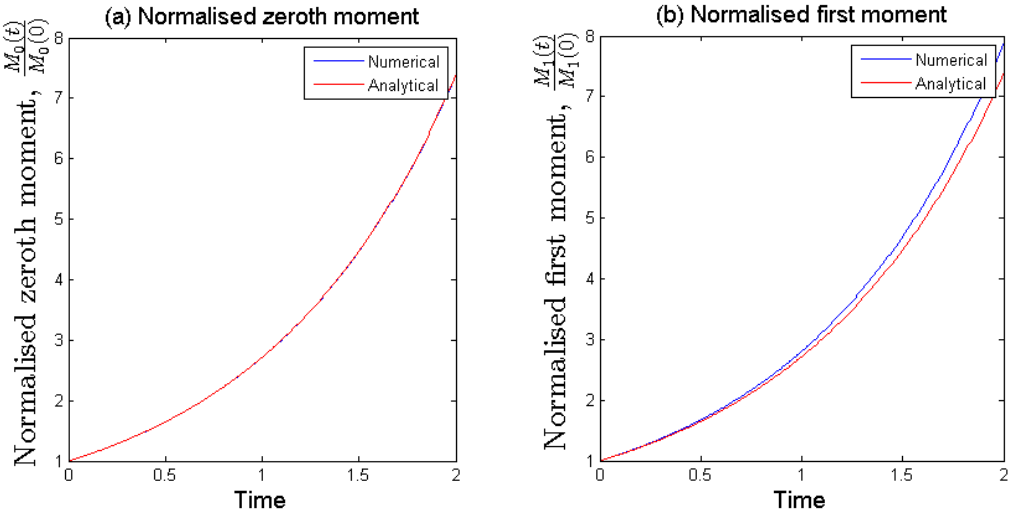

Figure 6: Comparison of the numerical and analytical solutions of the (a) zeroth and (b) first normalised moments using 300 grid points.

4.2 Unimodal kernels

Throughout the remainder of this section, we will focus on the biological problem discussed previously, and vary the choice of breakage kernel, $p(x, y)$, to analyse

the affect this has on the cluster size distribution. The values for all the other parameters used throughout this section are fixed based on the biological problem. We take $c = 7 \times 10^{-5}$ and $g(x) = x$, which will result in exponential growth and the rate of growth is the same as the rate of monomeric binding as discussed earlier. This has been chosen to reflect the expected exponential growth in the absence of inhibitors such as low nutrient levels. The selection function, $s(x)$, is taken to be

$$s(x) = \begin{cases} 0, & \text{if } x < 10^4, \\ 10^{-3}, & \text{otherwise.} \end{cases}$$

This stepwise function has been chosen based on the nature of the observed splitting process, as described earlier, whereby the cluster cannot split until it has reached a certain value, $x_{\text{split}} = 10^4$, and after this size has been reached the selection function will allow splitting to occur at a uniform rate $\gamma = 10^{-3}$. Furthermore, to reduce the error from the numerical method, 300 grid points will be used throughout with the grid generated as in (32), but here we will take $[v_{\min}, v_{\max}] = [10^3, 3 \times 10^4]$ and the maximum time is taken to be $t_{\max} = 4 \times 10^4$.

The initial condition is taken to be a normal distribution for $n(x, 0)$, and therefore for $N_i(0)$, the initial condition is given by

$$\begin{aligned} N_i(0) &= \int_{v_i}^{v_{i+1}} \frac{1}{\sqrt{2\pi}\sigma} e^{\frac{-(x-\mu)^2}{2\sigma^2}} \\ &= -\frac{1}{2}\text{erf}\left(\frac{\mu - v_{i+1}}{\sigma\sqrt{2}}\right) + \frac{1}{2}\text{erf}\left(\frac{\mu - v_i}{\sigma\sqrt{2}}\right), \end{aligned} \tag{33}$$

where $\text{erf}(x)$ is the error function,

$$\text{erf}(x) = \frac{2}{\sqrt{\pi}} \int_0^x e^{-t^2} dt.$$

The kernels considered here belong to the two-parameter family

$$p(x, y) = \left(\frac{1}{\frac{x}{y} + b} + \frac{1}{1 - \frac{x}{y} + b} + \frac{2(g-1)}{b + 0.5}\right) \frac{I}{y}, \tag{34}$$

with

$$I = \frac{0.5}{\ln(1+b) - \ln(b) + \frac{g-1}{b+0.5}},$$

and where g is given by

$$g = \frac{0.5a}{2b(1+b)(1-a)}.$$

This kernel is shown, for the parameter choices we will be considering, in Fig. 7 below.

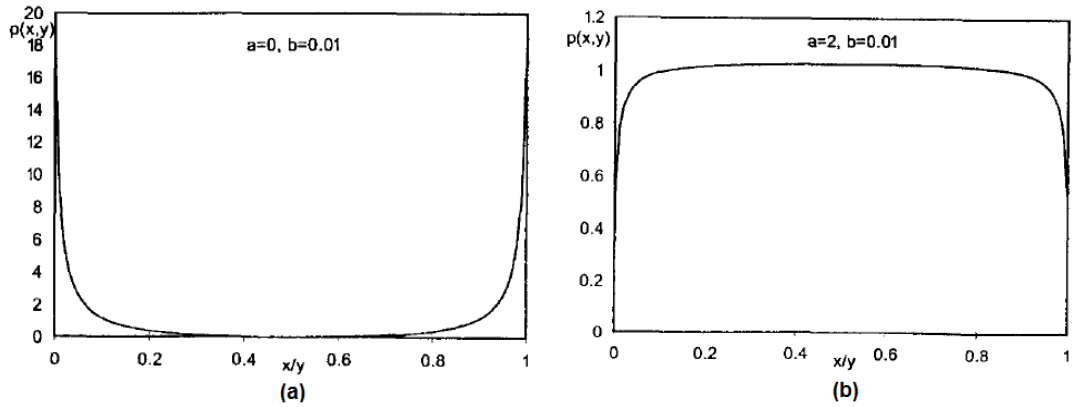

Figure 7: Unimodal kernels for chosen parameter values [8].

First, taking $a = 0$ and $b = 0.01$, we expect a large number of clusters near 0 and near x_{split} when splitting occurs, and none in between (giving a bimodal structure) as $p(x, y)$ is large when $\frac{x}{y}$ is near 0 or near 1. We can plot the zeroth and first moments (Fig. 8) and the cluster size distribution (Fig. 9).
We can see that the normalised zeroth moment (number of clusters) rapidly increases at a time corresponding to the splitting event being triggered by cluster sizes greater than x_{split} and the first moment evolves exponentially, as would be expected.

From Fig. 9 we can see that the cluster size distribution is clearly bimodal, with a peak at a low cluster size, which can be interpreted as the daughter cells, and a peak near $x_{\text{split}} = 10^4$. The distribution decreases after this point, as we would expect since the clusters of this size will then have a constant non-zero probability of splitting introduced by the selection function $s(x)$. However, the majority of parent clusters have size greater than x_{split}, which is not expected from the biological observations. When a cluster of size $x \geq x_{\text{split}}$ splits, it will create a daughter cluster of size x_0 and a parent cluster of size $x - x_0$. We therefore

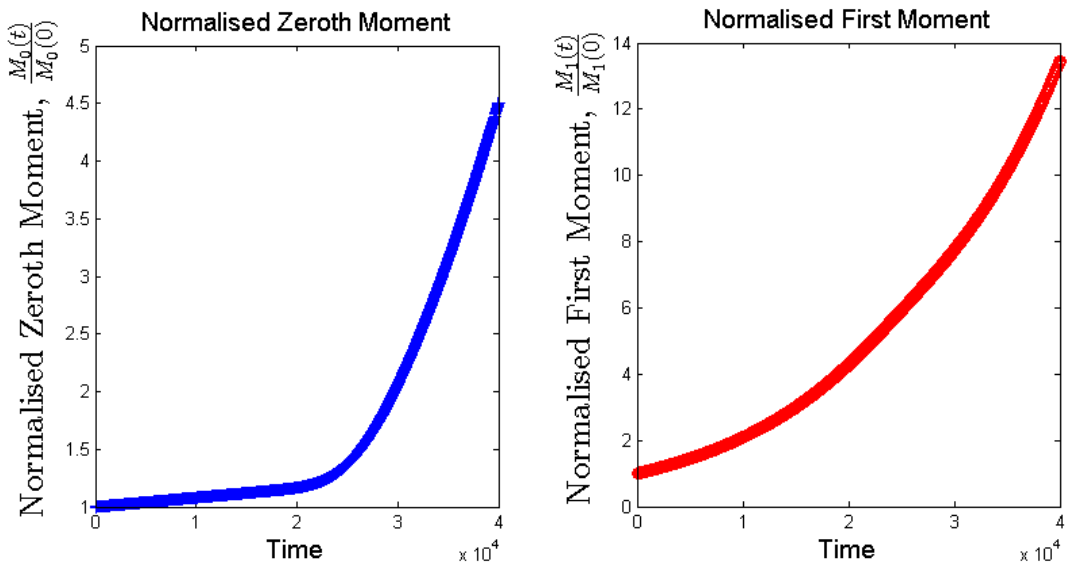

Figure 8: Normalised zeroth and first moments using (34) with $a = 0$ and $b = 0.01$.

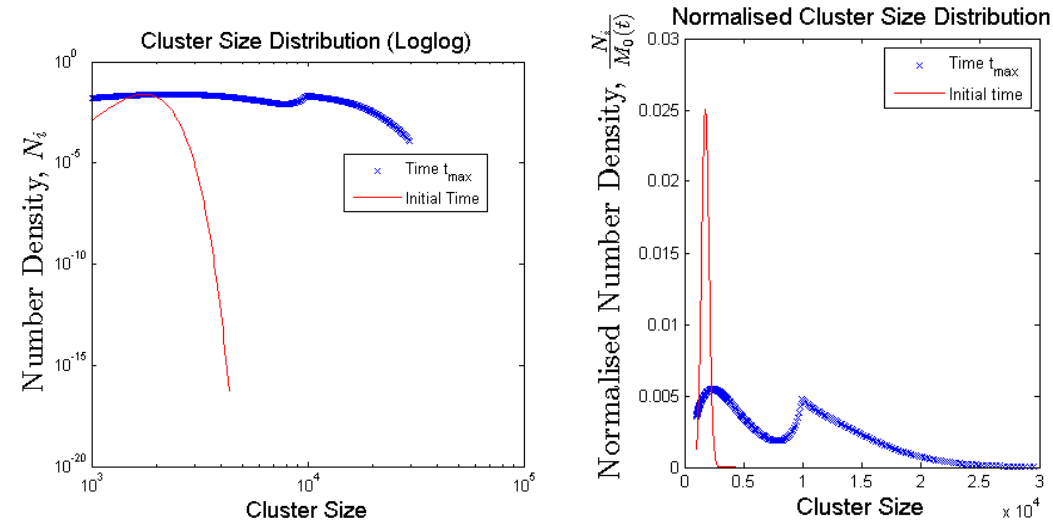

Figure 9: Cluster size distribution plotted on a log-log scale and normalised cluster size distribution for $a = 0$ and $b = 0.01$.

expect the size of the parent cluster to generally be less than x_{split}, and so would expect to see two modes at cluster sizes below x_{split}, indicating that a unimodal kernel (34) with $a = 0$ and $b = 0.01$ is not an appropriate choice for our biological problem.

However, we can analyse the cluster size distribution for the existence of a stable

size distribution by plotting the distribution at a number of equally spaced times between 0 and $t_{\max}$. With the current choice of $t_{\max}$, a stable size distribution is not yet apparent, however by setting $t_{\max} = 1.6 \times 10^5$, we get

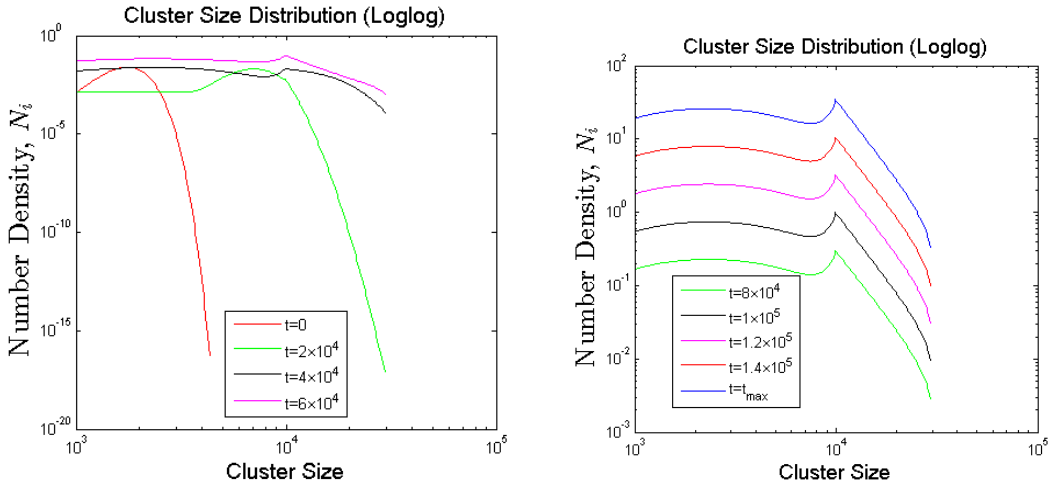

Figure 10: Cluster size distribution plotted on a loglog scale for unimodal kernel (34) with $a = 0$ and $b = 0.01$ at equally distributed times.

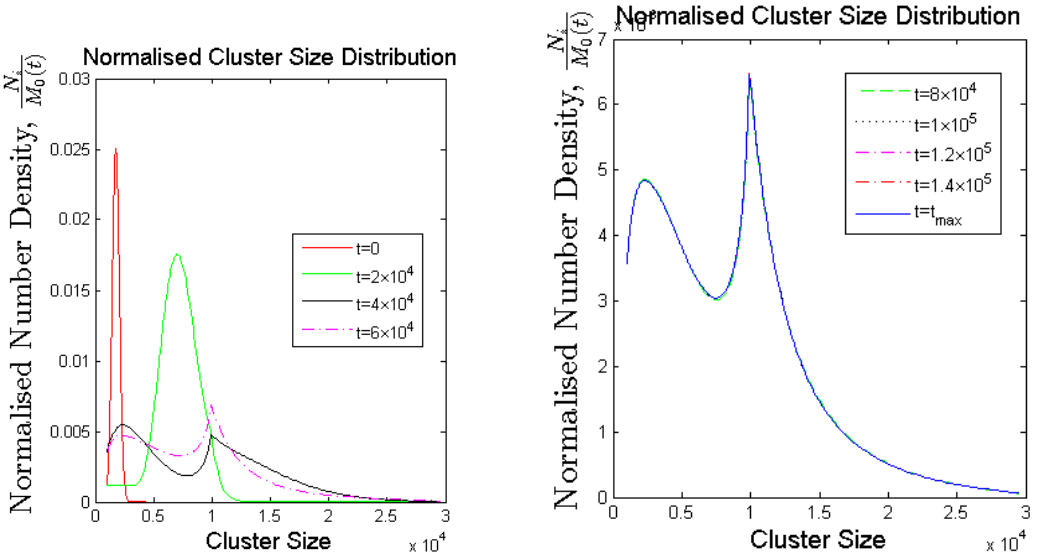

Figure 11: Normalised cluster size distribution for unimodal kernel (34) with $a = 0$ and $b = 0.01$ at equally distributed times.

Fig. 10 shows a clear stable size distribution, with an exponential increase in the number density, while Fig. 11 shows that once a stable size distribution is reached, the shape of the distribution does not change.

In an attempt to reduce the chance of small daughter clusters and large parent clusters after splitting we consider the choice of parameters $a = 2$ and $b = 0.01$, as shown in Fig. 34(b) for which there is a uniform distribution with exceptions near $\frac{x}{y} = 0$ and $\frac{x}{y} = 1$, and so there is no mechanism provided by the breakage kernel to create a difference in size between the daughter and parent clusters. We can again plot the normalised moments (Fig. 12) and cluster size distribution (Fig. 13).

The normalised zeroth and first moments behave similarly as to the case with

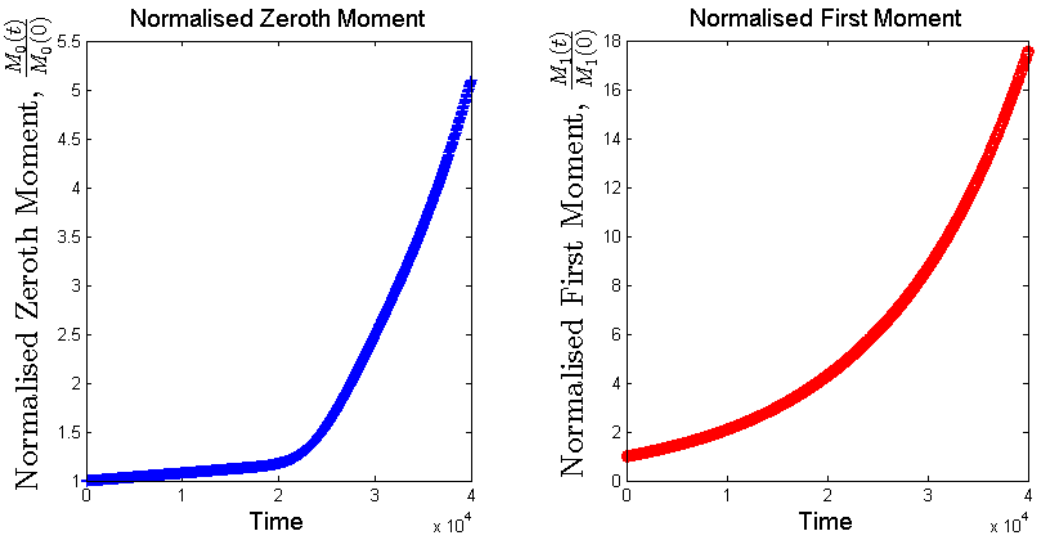

Figure 12: Normalised zeroth and first moments using kernel (34) with $a = 2$ and $b = 0.01$.

$a = 0$ and $b = 0.01$, with a rapid increase after the splitting events begin in the zeroth moment and exponential growth of the first moment.

However, the cluster size distribution shown in Fig. 13 no longer has a bimodal shape. In the previous case, the choice of breakage kernel appeared to produce too large a parent cluster after the split, whereas this choice appears to be lacking differentiation in size between the daughter and parent clusters as there is only one peak, just below x_{split}. We can infer from this that the unimodal kernel (34) with $a = 2$ and $b = 0.01$ is also not an appropriate choice for our problem.

We can however again look for a stable size distribution by setting $t_{\max} = 1.6 \times 10^5$

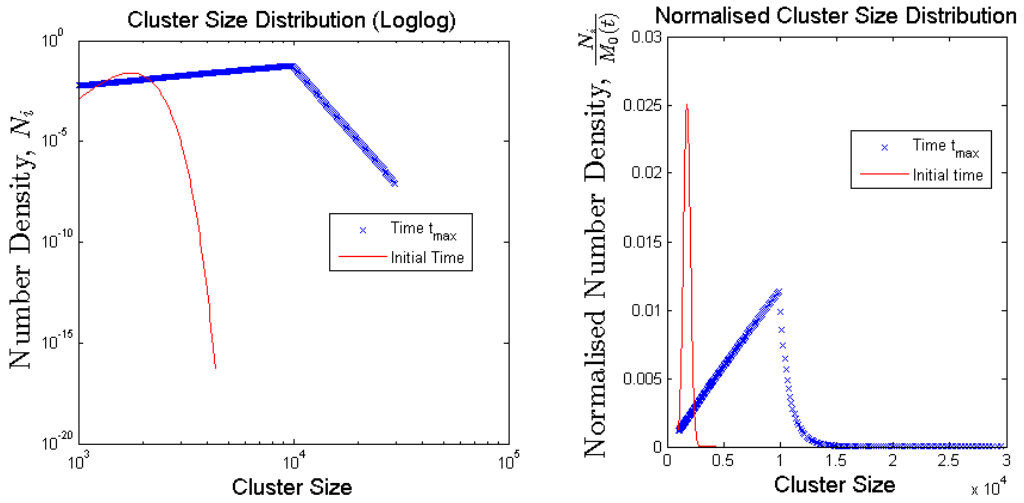

Figure 13: Cluster size distribution plotted on a loglog scale and normalised cluster size distribution for $a = 2$ and $b = 0.01$.

and plotting the distribution at evenly distributed times, As for the previous

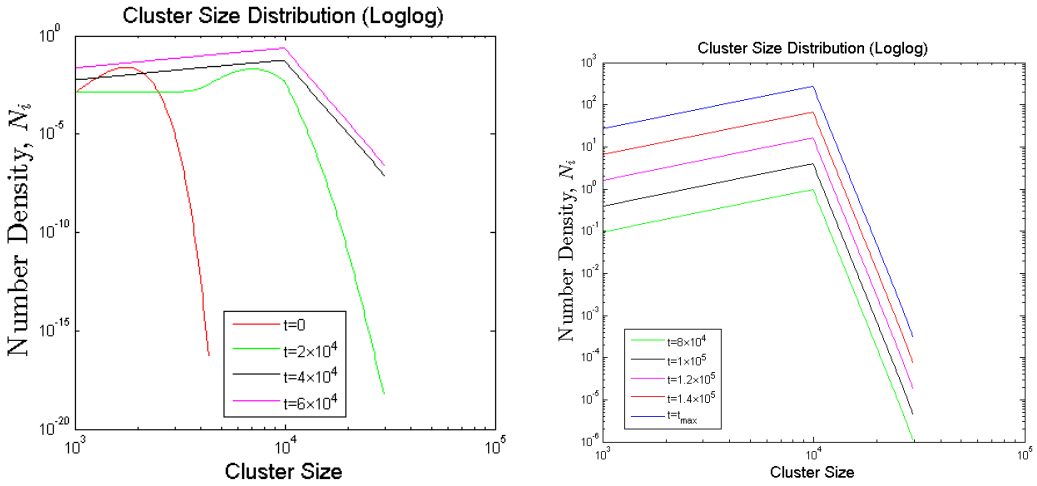

Figure 14: Cluster size distribution plotted on a loglog scale for unimodal kernel (34) with $a = 2$ and $b = 0.01$ at equally distributed times.

kernel choice, Fig. 14 clearly shows a stable size distribution with exponential increase in the number density and Fig. 15 shows that the normalised cluster size distribution remains exactly the same shape once stable.

To find a better fitting kernel, we would like to take some desirable qualities from these two unimodal kernels, namely that $p(x, y)$ is very low near $\frac{x}{y} = 0$ and $\frac{x}{y} = 1$, so that when splitting occurs, the parent cluster should be smaller than x_{split}, and

that $p(x, y)$ is non-zero for some other choices of $\frac{x}{y}$.

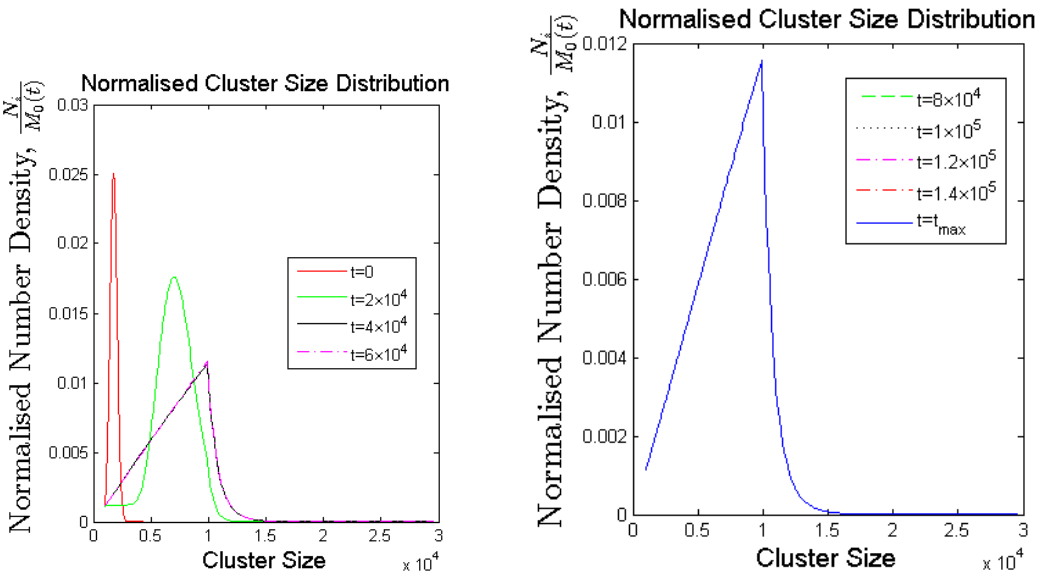

Figure 15: Normalised cluster size distribution for unimodal kernel (34)with $a = 2$ and $b = 0.01$ at equally distributed times.

4.3 A bimodal kernel

To produce an appropriate size distribution for our problem, we consider a bimodal kernel, which is given by

$$p(x, y) = \frac{1}{2} \left(p_1(x, y) + p_2(x, y) \right), \tag{35}$$

where

$$p_1(x, y) = f\left(\frac{x}{y}; \mu, \sigma\right) = \frac{1}{\sigma\sqrt{2\pi}\frac{x}{y}\left(1 - \frac{x}{y}\right)} \exp\left(\frac{-\left(\text{logit}(\frac{x}{y} - \mu)\right)^2}{2\sigma^2}\right), \tag{36}$$

and

$$p_2(x, y) = f\left(\frac{x}{y}; -\mu, \sigma\right) = \frac{1}{\sigma\sqrt{2\pi}\frac{x}{y}\left(1 - \frac{x}{y}\right)} \exp\left(\frac{-\left(\text{logit}(\frac{x}{y} + \mu)\right)^2}{2\sigma^2}\right), \tag{37}$$

where $f(x, \mu, \sigma)$ is the probability density function of the logit-normal distribution where $\text{logit}(x) = \ln(\frac{x}{1-x})$ and μ and σ are the mean and standard deviation of

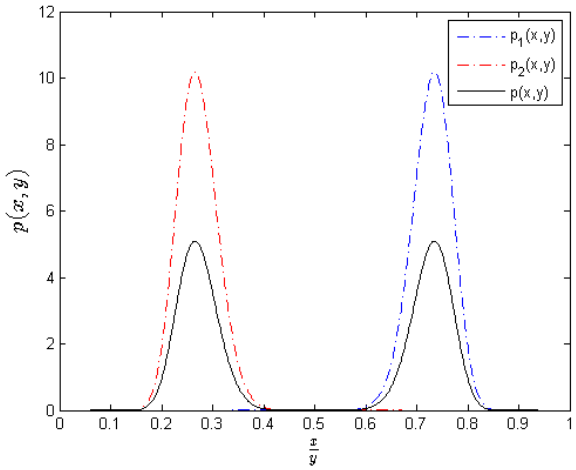

Figure 16: Bimodal kernel (35) created using two logit normal distributions (36) and (37), with parameters $\mu = 1$ and $\sigma = 0.2$.

the variable's logit. This kernel is plotted in Fig. 16 with $\mu = 1$ and $\sigma = 0.2$.

Using the same parameter values for $c, g(x)$ and $s(x)$ as before and generating the grid as before (32) with $[v_{\min}, v_{\max}] = [10^3, 3 \times 10^4]$, with the same initial condition as for the unimodal kernels (33), the normalised moments can be plotted (Fig. 17). Although the normalised moments do not immediately appear similar

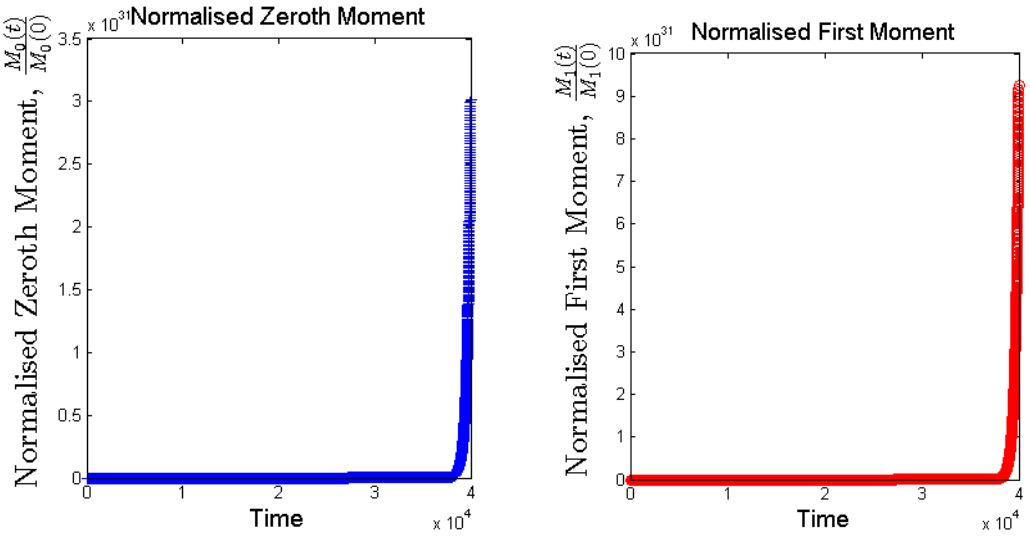

Figure 17: Normalised zeroth and first moments for the bimodal kernel (35) with $\mu = 1$ and $\sigma = 0.2$.

to the results from the unimodal kernels, they can be plotted on a log-linear scale

(Fig. 18), from which we can see that both the zeroth moment and first moments are growing exponentially once the splitting event has been triggered.

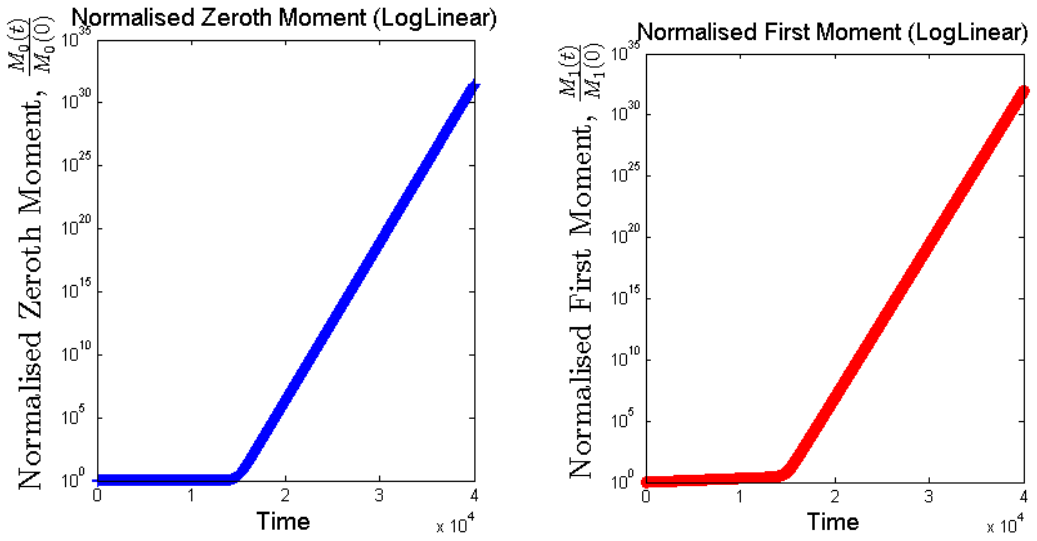

Figure 18: Normalised zeroth and first moments for the bimodal kernel (35) with $\mu = 1$ and $\sigma = 0.2$ plotted on a log-linear scale.

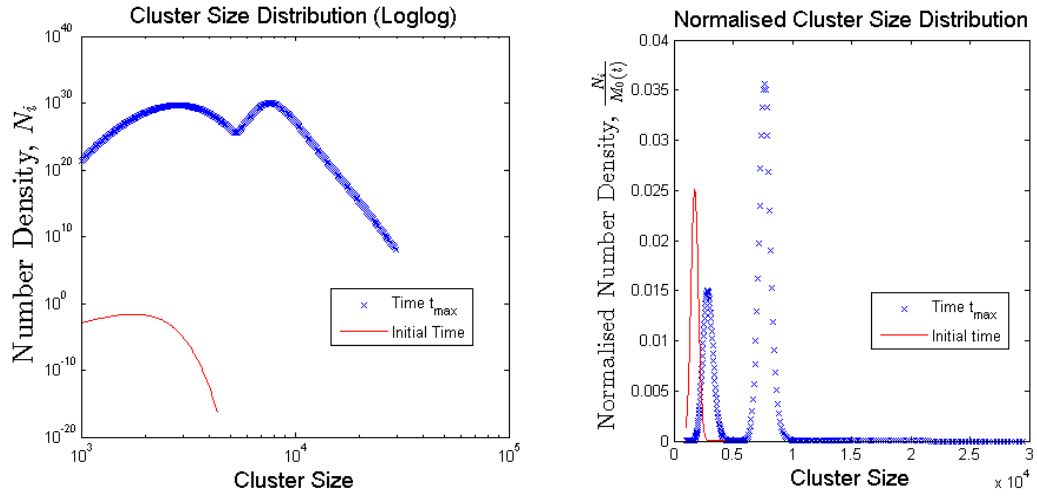

Figure 19: Cluster size distribution plotted on a loglog scale and normalised cluster size distribution for the bimodal kernel (35) with $\mu = 1$ and $\sigma = 0.2$.

The bimodal kernel (35) produces a bimodal cluster size distribution (Fig. 19), where one mode represents the daughter clusters and the mode just below x_{split} represents the parent clusters immediately after splitting. There are some clusters with size greater than x_{split}, but the majority larger than this will have split, creating the two modes. In fact, this cluster size distribution appears to accurately

describe the biological process, with very few clusters larger than x_{split}, and two modes representing the daughter clusters and the parent clusters after splitting.

We can show that this distribution is a stable size distribution by plotting the cluster size distribution at a number of evenly spaced times between the initial time and the final time, $t_{\max}$. This is shown in Fig. 20 and Fig. 21.

A stable size distribution can be clearly seen here; although the distribution is

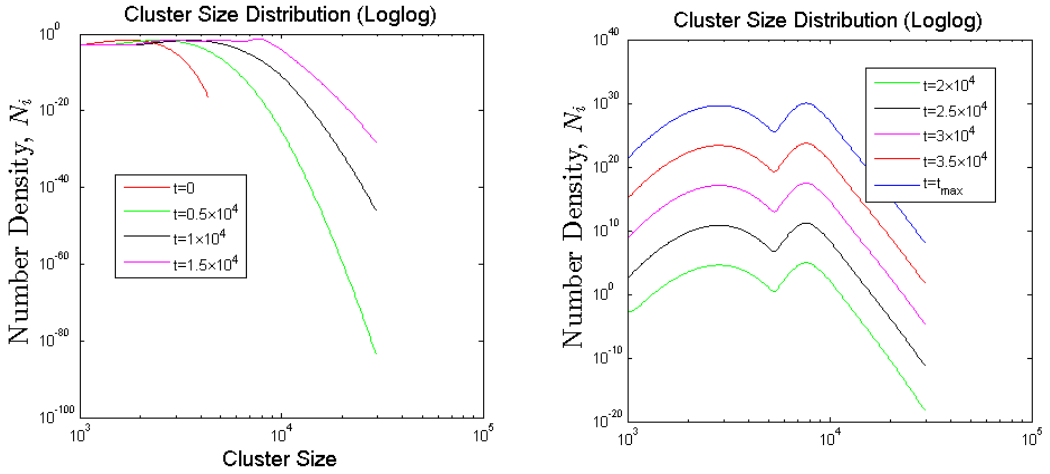

Figure 20: Cluster size distribution plotted on a loglog scale for bimodal kernel (35) with $\mu = 1$ and $\sigma = 0.2$ at equally distributed times.

increasing exponentially, this is what is expected from hyphal growth in the absence of inhibitors such as a lack of nutrients. By normalising the distribution, it clearly remains exactly the same shape once stable (Fig. 21). The bimodal kernel (35) reaches a stable size distribution much faster than the unimodal kernels (34), for which $t_{\max}$ had to be increased to find evidence of a stable size distribution.

5 Conclusions

A growth-fragmentation model describing the binding and splitting process of DivIVA molecules in *S.coelicolor* has been proposed, along with an appropriate sectional numerical method for the model. This numerical method comprises an upwind scheme for growth and a fixed pivot scheme for splitting. Compari-

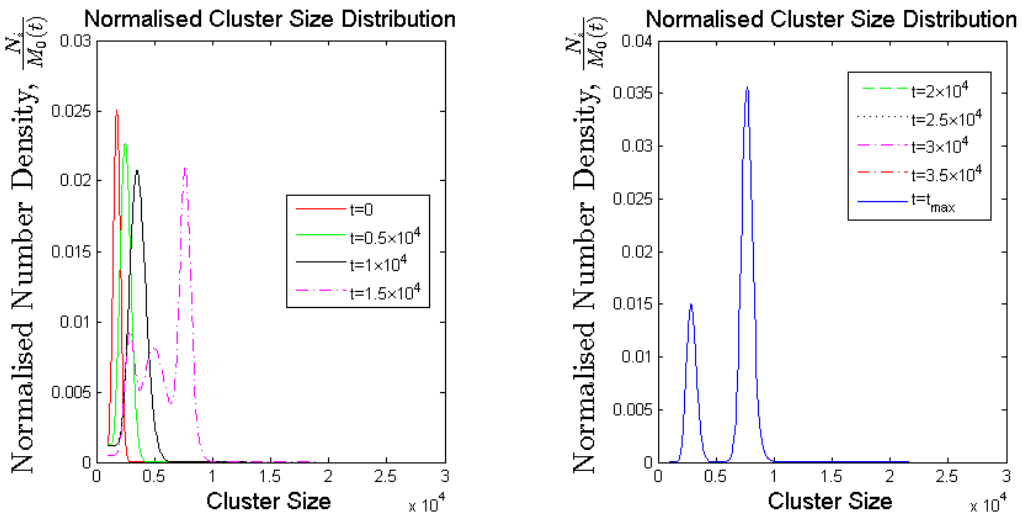

Figure 21: Normalised cluster size distribution for bimodal kernel (35)with $\mu = 1$ and $\sigma = 0.2$ at equally distributed times.

son of the numerical method with known analytical solutions has shown that the method is sufficiently accurate when an appropriate number of grid points is used.

We believe that much of the error is introduced through the use of the midpoint quadrature rule to evaluate integrals used in the fixed pivot method. Interesting further work could include finding analytical solutions for these integrals and again comparing the numerical method with analytical solutions when there is no error introduced through the midpoint rule.

The numerical method was then applied to two unimodal kernels. Although both of the unimodal kernels produced a stable size distribution in finite time, the distributions did not appear to replicate the experimental observations of the biological problem and so the two unimodal kernels are not appropriate choices for our problem. To find an appropriate kernel choice, desirable properties from the unimodal kernels were combined into a bimodal kernel. Again, a stable size distribution was reached in finite time and for the bimodal kernel the time required for convergence to a stable size ditribution was greatly reduced. Furthermore, by choosing a bimodal kernel the steady size distribution appears to reflect experimental observations.

To further develop this model, the effect of nutrient levels could be included and the existence of a steady state size distribution could be proven analytically [7]. Additionally, if experimental data on cluster size distributions was to be gathered from imaging of *S.coelicolor* growth with the DivIVA protein tagged, the the steady size distribution could be compared with the size distribution of the imaged DivIVA clusters. Biologists in the Polarised Growth VIP team are currently imaging DivIVA clusters, and we hope that cluster size information will be extracted using image processing techniques to give an accurate distribution for comparison.

References

[1] http://www.jic.ac.uk/science/molmicro/strept.html Accessed June 1, 2015.

[2] Bentley, S.D., Chater, K.F., Cerdeño-Tárraga, A.-M., Challis, G.L., Thomson, N.R., James, K.D., Harris, D.E., Quail, M.A., Kieser, H., Harper, D., et al. (2002) Complete genome sequence of the model actinomycete *Streptomyces coelicolor* A3(2). *Nature.* **417** (6885), 141–147.

[3] Wolánksi, M., Wali, R., Tilley, E., Jakimowicz, D., Zakrzewska-Czerwińska, J. & Herron, P. (2011) Replisome trafficking in growing vegetative hyphae of *Streptomyces coelicolor* A3(2). *Journal of bacteriology.* **193** (5), 1273–1275.

[4] Flärdh, K. (2010) Cell polarity and the control of apical growth in *Streptomyces. Current opinion in Microbiology.* **13** (6), 758–765.

[5] Richards, D.M., Hempel, A.M., Flärdh, K., Buttner, M.J. & Howard, M. (2012) Mechanistic basis of branch-site selection in filamentous bacteria. *PLoS Computational Biology.* **8** (3) e1002423 .

[6] Richards, D.M., Hempel, A.M., Flärdh, K., Buttner, M.J. & Howard, M. (2012) Regulation of apical growth and hyphal branching in *Streptomyces. Current opinion in Microbiology.* **15** (6), 737–743.

[7] Heijmans, H. J. A. M. (1984) On the stable size distribution of populations reproducing by fission into two unequal parts. *Mathematical biosciences*. **72** (1), 19–50.

[8] Kostoglou, M., Dovas, S. & Karabelas, A.J. (1997) On the steady-state size distribution of dispersions in breakage processes. *Chemical Engineering Science*. **52** (8), 1285–1299.

[9] Doumic, M. & Tine, L.M. (2013) Estimating the division rate for the growth-fragmentation equation. *Journal of Mathematical Biology*. **67** (1), 69–103.

[10] Bell, G.I. & Anderson, E.C. (1967) Cell growth and division: I. a mathematical model with applications to cell volume distributions in mammalian suspension cultures. *Biophysical Journal*. **7**(4), 329–351.

[11] Pakdaman, K., Perthame, B. & Salort, D. (2013) Relaxation and self-sustained oscillations in the time elapsed neuron network model. *73*(3), 1260–1279.

[12] Calvez, V., Lenuzza, N., Oelz, D., Deslys, J-P., Laurent, P., Mouthon, F. & Perthame, B. (2009) Size distribution dependence of prion aggregates infectivity. *Mathematical Biosciences*. **817**(1), 88–99.

[13] Kumar, S. & Ramkrishna, D. (1996) On the solution of population balance equations by discretization – I. a fixed pivot technique. *Chemical Engineering Science*. **51** (8), 1311–1322.

[14] Kumar, R., Kumar, J. & Warnecke, G. (2013) Moment preserving finite volume schemes for solving population balance equations incorporating aggregration, breakage, growth and source terms. *Mathematical Models and Methods in Applied Sciences*. **23**(7), 1235–1273.

[15] Kumar, J., Peglow, M., Warnecke, G. & Heinrich,S. (2008) An efficient numerical technique for solving population balance equation involving aggregation, breakage, growth and nucleation. *Powder Technology*. **182**(1), 81–104.

[16] Kumar, J. & Warnecke, G. (2008) Convergence analysis of sectional methods for solving breakage population balance equations -I: the fixed pivot technique. *Numerische Mathematik*. **110**(4), 539–559.

[17] Hundsdorfer, W. & Verwer, J.G. Numerical solution of time-dependent advection-diffusion-reaction equations, 1st edition. Springer, New York (2003).